

The BoRG-*JWST* Survey: Analogs at $z \sim 8$ to the UV-luminous Galaxy Population at $z \gtrsim 10$

SOFÍA ROJAS-RUIZ ¹ GUIDO ROBERTS-BORSANI ² TAKAHIRO MORISHITA ³ ANTONELLO CALABRÒ ⁴
MICAELA BAGLEY ⁵ TOMMASO TREU ¹ STEVEN L. FINKELSTEIN ⁵ MASSIMO STIAVELLI ^{6,7,8} MICHELE TRENTI ⁹
AND L. Y. AARON YUNG ⁶

¹*Department of Physics and Astronomy, University of California, Los Angeles, 430 Portola Plaza, Los Angeles, CA 90095, USA*

²*Department of Physics & Astronomy, University College London, London, WC1E 6BT, UK*

³*IPAC, California Institute of Technology, MC 314-6, 1200 E. California Boulevard, Pasadena, CA 91125, USA*

⁴*INAF-Osservatorio Astronomico di Roma, via di Frascati 33, 00078 Monte Porzio Catone, Italy*

⁵*Department of Astronomy, The University of Texas at Austin, 2515 Speedway, Austin, TX, 78712, USA*

⁶*Space Telescope Science Institute, 3700 San Martin Drive, Baltimore, MD 21218, USA*

⁷*Dept. of Physics & Astronomy, Johns Hopkins University, Baltimore, MD 21218, USA*

⁸*Dept. of Astronomy, University of Maryland, College Park, MD 20742, USA*

⁹*School of Physics, University of Melbourne, Parkville 3010, VIC, Australia*

ABSTRACT

The population of bright galaxies at $z \gtrsim 10$ discovered by *JWST*, including the so-called “blue monsters”, has been difficult to reconcile with standard galaxy evolution models. To shed light on this extraordinary population, we study the $z \sim 8$ galaxies discovered by the BoRG-*JWST* survey. These slightly-lower redshift analogs are comparable in UV luminosity to the blue monsters, and their lower redshift makes it much easier to access key rest frame optical diagnostics with NIRspec. We find that BoRG-*JWST* galaxies are consistent with being dust-poor based on their blue UV slopes and Balmer decrement ratios. We find no strong evidence for dominant active galactic nuclei contribution to the UV brightness, based on line-ratio diagnostics, though some contribution cannot be excluded. We further infer the stellar mass, star formation and UV-brightness history of the BoRG-*JWST* galaxies by fitting their rest-frame UV-optical spectra. We see evidence for stochastic episodes of star formation for all the BoRG-*JWST* galaxies, providing a temporal boosting of UV luminosity in short timescales. The UV-bright blue monsters at $z \gtrsim 10$ can be explained by the presence of stars with ages below 100 Myr.

Keywords: galaxies: high-redshift, star formation, active galactic nuclei - cosmology: observations

1. INTRODUCTION

It took just a few days for the *JWST* Near-Infrared Camera (NIRcam; 0.6–5 μ m) to force a revision on our understanding of early galaxy formation by discovering numerous candidate bright galaxies at $z \gtrsim 10$ (e.g., Castellano et al. 2022; Finkelstein et al. 2022; Naidu et al. 2022). Multiple studies have since confirmed the existence of this population of intrinsically UV-luminous galaxies ($M_{UV} < -20$; e.g., Naidu et al. 2022; Castellano et al. 2023; Curtis-Lake et al. 2023; Finkelstein et al. 2023, 2024; Harikane et al. 2023; Robertson et al. 2024; Hainline et al. 2024). These galaxies have very blue UV-

continuum slopes (β_{UV}), with indications of “dust-free” or essentially no dust attenuation for $z \gtrsim 11$ galaxies investigated in Cullen et al. (2024). Additionally, the $z > 10$ UV-luminous population appears to have intermediate to high stellar masses of $\sim 10^8 - 10^9 M_{\odot}$ (e.g., Bunker et al. 2023; Carniani et al. 2024; Castellano et al. 2024; Naidu et al. 2025), with extreme cases pushing the limits of early mass assembly (e.g., Casey et al. 2024). This population of massive UV-bright galaxies has been aptly nicknamed “blue monsters” to describe their extreme properties (e.g., Ziparo et al. 2023; Ferrara 2024a; Ferrara et al. 2025).

Three broad classes of mechanisms have been proposed to explain the extreme properties observed in blue monsters: (i) The lack of dust, which could be explained by ejection due to radiation pressure or segre-

gated with respect to UV-emitting regions (Ferrara et al. 2023, 2025; Ziparo et al. 2023). Some studies have already favored the dust ejection case given non-detection of dust continuum at sensitive wavelengths tracing dust emission in these UV-luminous galaxies (Bakx et al. 2023; Fujimoto et al. 2023; Carniani et al. 2025). (ii) The nature of the source and mechanisms responsible for removing dust from these early galaxies. Fiore et al. (2023) proposed radiative outflows clearing dust in the galaxy that could be produced by the presence of active galactic nuclei (AGN) (Bunker et al. 2023; Maiolino et al. 2024a,b), low-metallicity stellar populations (Ferrara 2024a), or dual AGN and strong star formation contributing to the emission (Calabrò et al. 2024; Napolitano et al. 2024). (iii) Stochastic star formation and thus young stellar ages at the time of observations can explain the extreme luminosity (Mason et al. 2023; Casey et al. 2024; Dressler et al. 2023, 2024; Gelli et al. 2024).

Importantly, however, *JWST*-NIRSpec observations (0.6–5.3 μm) which have spectroscopically confirmed blue monsters at $z > 10$ only probe their rest-frame UV emission. To further investigate the formation and evolution of these UV-luminous galaxies, access to their rest-frame optical emission is necessary (i.e., with MIRI $> 5\mu\text{m}$ Ferrara 2024a). In fact, thus far, just three of these blue monsters have been followed up with MIRI to analyze the [O III] $\lambda\lambda 4959, 5007$, and H α emission lines (MACS0647-JD; $z=10.17$, Hsiao et al. 2024), (GN-z11; $z=10.60$, Álvarez Márquez et al. 2025), (GHZ2; $z=12.33$, Zavala et al. 2025). The difficult and time-consuming process of detecting the rest-optical emission at $z \gtrsim 10$ clearly exemplifies why it is very helpful to study lower redshift analogs.

The BoRG-*JWST* survey –Cy1 GO 1747 (PI: Roberts-Borsani) and GO 2426 (Co-PIs: Bagley and Rojas-Ruiz)– provides a sample of spectroscopically confirmed $z = 7 - 9$ galaxies that is robust against cosmic variance (Roberts-Borsani et al. 2025). The NIRSpec PRISM R = 3 – 300 resolution observations offer crucial information on the properties of these galaxies in the rest-UV and in the rest-optical spectrum. Roberts-Borsani et al. (2025) calculated the β_{UV} slopes and M_{UV} values of the BoRG-*JWST* galaxies at $z \sim 8$ and showed that they are in good agreement with the spectroscopically confirmed luminous $z > 10$ population. Furthermore, Rojas-Ruiz et al. (2025) found that the number density and scatter in the mass-to-light ratio of this sample supported a stochastic star formation scenario. Thus, the BoRG-*JWST* galaxies are indicative of being ideal analogs to the $z \gtrsim 10$ blue monster population based on their intrinsic UV properties.

In this paper, we use BoRG-*JWST* galaxy spectra as analogs to the $z > 10$ blue monsters to investigate the physical mechanisms driving the formation of UV-bright, massive galaxies. We describe the data and fitting methodologies to measure emission lines and model star formation histories in §2. We use the β_{UV} and Balmer decrement H δ /H β diagnostics to investigate dust extinction in §3.1. We present the OHNO diagnostic to evaluate the AGN vs. strong star-forming engine responsible for the extreme UV emission observed in §3.2. Lastly, in §3.3 we present their stellar mass, star formation history and UV luminosity as a function of lookback time to identify bursty episodes of star formation. In §3.4 we summarize our findings and highlight the rest-optical properties of BoRG-*JWST* galaxies that are key to understand blue monsters.

Throughout this work, we use the cosmology according to $H_0 = 70 \text{ km s}^{-1} \text{ Mpc}^{-1}$, $\Omega_m = 0.3$, and $\Omega_\Lambda = 0.7$ and a Chabrier (2003) initial mass function (IMF). All magnitudes are given in the AB system.

2. DATA AND METHODS

The spectral information offers a holistic assessment of the dust content, ionizing nature, and star formation history responsible for producing these massive UV-bright galaxies. We use the reduced NIRSpec spectra of the BoRG-*JWST* galaxies as described by Roberts-Borsani et al. (2025), hereafter RB25. The analysis is divided into emission line diagnostics and modeling of their spectra.

2.1. Emission Line fit

We divide the spectrum of each galaxy into three rest-frame spectral windows: (1) the rest-UV covering emission lines C IV $\lambda\lambda 1548, 1550$ to C III] $\lambda\lambda 1907, 1909$; (2) rest-optical spanning [O II] $\lambda\lambda 3726, 3729$ to H γ + [O III] $\lambda 4363$; and (3) a second rest-optical window covering H β $\lambda 4861$ through [O III] $\lambda\lambda 4959, 5007$. We use the `astropy.modeling` package to fit the emission lines using Gaussian profiles. We perform bootstrap resampling 100 times where in each step the spectrum is perturbed with Gaussian noise. The code iterates over each spectral window on the same noisy realization of the spectrum and computes the line fluxes with the underlying continuum. The minimum signal-to-noise ratio (S/N) required for emission line detection is $S/N > 2.5$. We also measure the line ratio of H δ /H β that is used for dust attenuation analysis in §3.1, and the ratios Ne III $\lambda 3870$ /[O II] $\lambda\lambda 3726, 3729$ and [O III] $\lambda 5007$ /H β to identify the type of ionizing source in §3.2. The uncertainties in the emission line fluxes and ratios are calculated from the 16th and 84th percentiles of the

Table 1. Properties of the BoRG-*JWST* galaxies

ID	z	M_{UV}	β_{UV}	[O II] $\lambda\lambda 3726, 29$	[O III] $\lambda 5007$	H_δ/H_β	Ne3O2	R3	$\log_{10} M_*/M_\odot$
				10^{-18} [cgs]	10^{-18} [cgs]				
1747_138	7.179	-21.42±0.16	-2.52 ± 0.05	1.03 ^{+0.21} _{-0.17}	7.45 ^{+0.28} _{-0.31}	0.33 ^{+0.10} _{-0.19}	-0.12 ^{+0.44} _{-0.18}	0.60 ^{+0.07} _{-0.05}	9.61 ^{+0.04} _{-0.06}
2426_112	7.337	-21.94±0.07	-2.41 ± 0.07	1.35 ^{+0.22} _{-0.19}	19.51 ^{+0.90} _{-0.87}	0.27 ^{+0.12} _{-0.12}	0.41 ^{+0.13} _{-0.18}	0.82 ^{+0.08} _{-0.06}	9.32 ^{+0.27} _{-0.25}
1747_1425	7.553	-21.38±0.06	-2.30 ± 0.07	1.36 ^{+1.09} _{-0.29}	16.29 ^{+0.35} _{-0.34}	—	0.13 ^{+0.24} _{-0.12}	0.85 ^{+0.13} _{-0.04}	9.86 ^{+0.11} _{-0.14}
1747_817	7.556	-20.74±0.13	-2.42 ± 0.09	2.69 ^{+0.26} _{-0.29}	20.59 ^{+0.37} _{-0.27}	0.15 ^{+0.18} _{-0.03}	-0.31 ^{+0.11} _{-0.07}	0.81 ^{+0.03} _{-0.01}	8.97 ^{+0.63} _{-0.16}
2426_1736	7.822	-20.65±0.14	-2.16 ± 0.15	2.81 ^{+0.64} _{-0.67}	14.16 ^{+0.32} _{-0.44}	0.22 ^{+0.19} _{-0.09}	-0.36 ^{+0.23} _{-0.19}	0.81 ^{+0.06} _{-0.06}	9.35 ^{+0.23} _{-0.21}
1747_1081	7.838	-21.59±0.14	-1.63 ± 0.06	1.82 ^{+0.36} _{-0.64}	4.37 ^{+0.25} _{-0.35}	—	—	0.50 ^{+0.18} _{-0.08}	9.59 ^{+0.24} _{-0.36}
1747_902	7.905	-21.10±0.19	-2.15 ± 0.09	2.00 ^{+0.30} _{-0.48}	16.92 ^{+0.31} _{-0.38}	0.16 ^{+0.10} _{-0.05}	-0.32 ^{+0.23} _{-0.12}	0.81 ^{+0.04} _{-0.04}	9.68 ^{+0.09} _{-0.45}
2426_1655	8.030	-20.68±0.19	-2.05 ± 0.13	3.44 ^{+0.72} _{-0.87}	27.67 ^{+0.59} _{-0.65}	0.24 ^{+0.20} _{-0.09}	-0.32 ^{+0.43} _{-0.16}	0.63 ^{+0.04} _{-0.04}	9.62 ^{+0.13} _{-0.13}
2426_169-n	8.205	-21.45±0.09	-2.50 ± 0.17	1.42 ^{+1.14} _{-0.33}	13.13 ^{+0.60} _{-0.48}	—	—	0.73 ^{+0.37} _{-0.13}	9.22 ^{+0.14} _{-0.08}
1747_732	8.226	-21.47±0.15	-2.21 ± 0.06	0.97 ^{+0.18} _{-0.26}	10.86 ^{+0.35} _{-0.34}	—	-0.17 ^{+0.57} _{-0.13}	0.88 ^{+0.10} _{-0.10}	9.75 ^{+0.06} _{-0.07}
2426_169	8.230	-22.34±0.06	-2.02 ± 0.10	2.10 ^{+0.36} _{-0.26}	66.07 ^{+0.59} _{-0.73}	0.19 ^{+0.04} _{-0.05}	0.43 ^{+0.13} _{-0.18}	0.73 ^{+0.03} _{-0.02}	10.09 ^{+0.03} _{-0.04}
1747_199	8.316	-21.28±0.17	-2.21 ± 0.06	1.47 ^{+0.26} _{-0.16}	11.05 ^{+0.33} _{-0.25}	0.13 ^{+0.04} _{-0.12}	-0.26 ^{+0.08} _{-0.09}	0.67 ^{+0.07} _{-0.05}	9.70 ^{+0.07} _{-0.19}
2426_1777	8.440	-20.44±0.41	-2.37 ± 0.36	0.89 ^{+0.58} _{-0.40}	12.85 ^{+0.43} _{-0.39}	—	—	0.71 ^{+0.09} _{-0.10}	9.72 ^{+0.32} _{-0.19}
2426_1130	8.490	-20.69±0.22	-2.37 ± 0.36	0.66 ^{+0.57} _{-0.66}	5.56 ^{+0.51} _{-0.55}	—	—	0.71 ^{+0.40} _{-0.14}	9.66 ^{+0.24} _{-0.22}

NOTE—Column 1: The galaxy named by observing program followed by ID. Columns 2–4 show the redshift, M_{UV} and β_{UV} values from RB25. Columns 5–6 show the [O II] $\lambda\lambda 3726, 29$ and [O III] $\lambda 5007$ emission line fluxes and errors in cgs units as calculated in §2.1. Column 7 has the H_δ/H_β Balmer ratios and errors. Columns 8–9 have the calculated Ne III $\lambda 3870$ /[O II] $\lambda\lambda 3726, 3729$ (Ne3O2) and [O III] $\lambda 5007/H_\beta$ (R3) line ratios and errors. Column 10 has the final stellar mass calculation from §2.2.

bootstrapped distributions. See Table 1 for the best-fit parameters of each BoRG-*JWST* galaxy.

2.2. Spectral Fitting

We perform spectral fitting on the full prism spectrum for each of the BoRG-*JWST* galaxies using the Grism SED fitter code `gsf` developed by members of our team (ver1.9.2 Morishita et al. 2019). This code is flexible to model multiple bursts or sudden declines in star formation history (SFH) using top-hat bins in age intervals. We can thus explore non-parametric SFHs to see evidence for bursty episodes of star formation that have been proposed as responsible mechanisms for the strong UV-brightness (M_{UV}) and high stellar masses of BoRG-*JWST* galaxies (Rojas-Ruiz et al. 2025), and of blue monsters (Ferrara et al. 2023).

The spectra are modeled by finding the best combination of composite stellar populations that match the observations. The model templates are generated from the `fsps` library (Conroy et al. 2009; Foreman-Mackey et al. 2013) taking metallicity and dust attenuation as free parameters with $\log Z_*/Z_\odot \in [-2, 0]$ in increments of 0.1, and $A_V \in [0, 4]$. We make a list of redshifts to sample the star formation history starting more densely closer to the age of the universe at the time the galaxy is observed and more sparsely earlier in time, in order to capture recent episodes with appropriate time resolu-

tion. In practice, this is achieved starting from the age of the universe at the time of observation and halving the interval multiple times. For example, for a galaxy at $z = 8.03$ with a corresponding age of the universe of 624 Myr, the grid of ages is [19, 39, 78, 156, 312, 624] Myr. We also add a nebular component characterized by $\log U \in [-3, -0.5]$ in increments of 0.5, which is included in the fitting process with a free amplitude parameter. The metallicity of the nebular component is set to that determined for the stellar template at the youngest age bin.

Through the spectral fitting we obtain the SFHs and the stellar mass of the galaxy ($\log M_*$) at the observed redshift, and at different lookback times. We also post-process the posterior SFH and recalculate the M_{UV} that the galaxy would have had if observed at earlier redshifts. This enables a more direct comparison to the observed M_{UV} of the $z \gtrsim 10$ UV-bright galaxies in the literature. For this calculation, we linearly sum the SED template at each lookback time to account for older stellar populations. At each lookback time, we scale the template based on the amount of stars that form in the previous age. This results in a cumulative SED that is used to calculate the UV luminosity and then the M_{UV} at each lookback time (see §3.3). We adopt the 16th

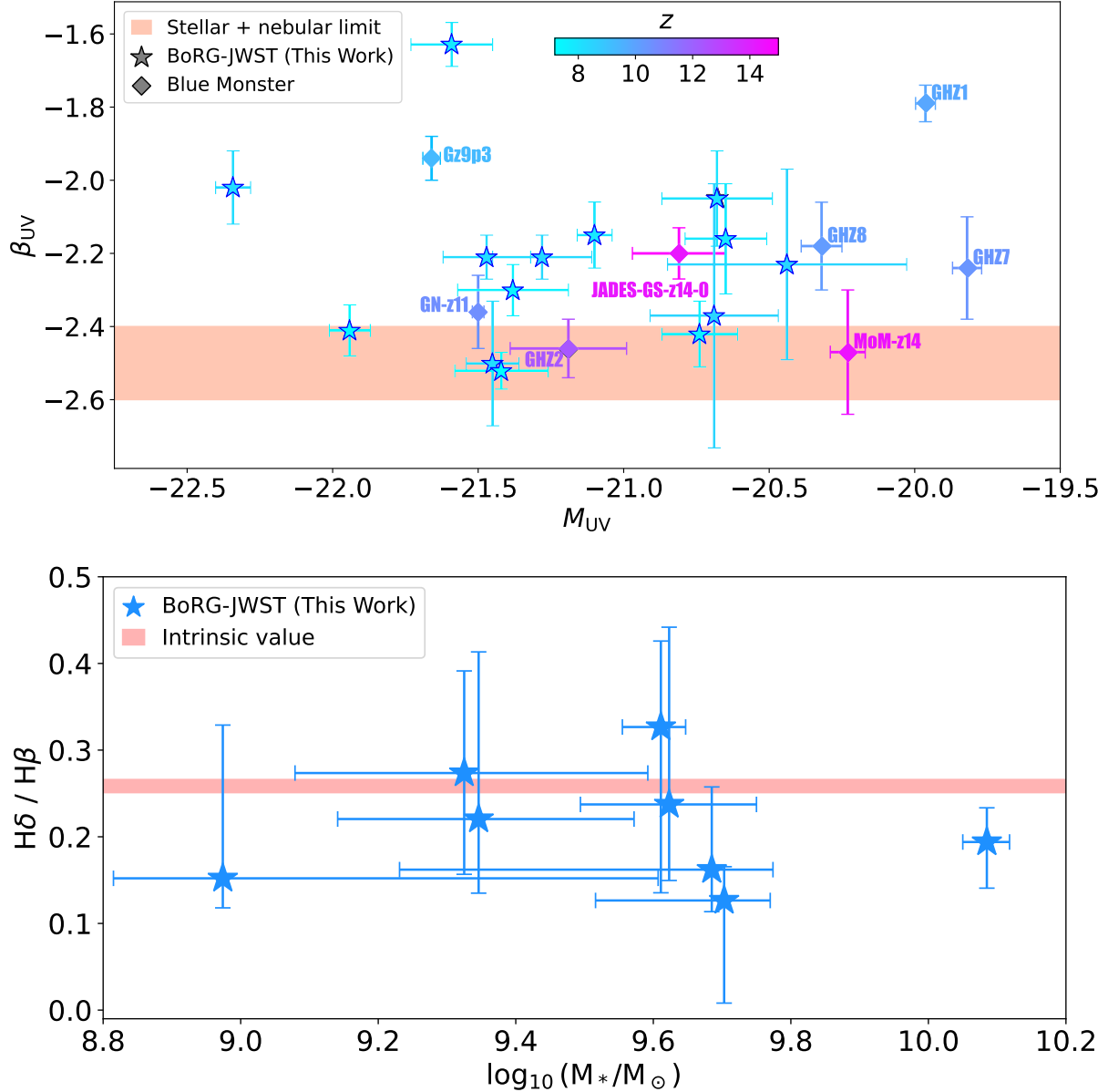


Figure 1. Evaluation of the dust content. *Top:* UV continuum β slope vs. UV magnitude of BoRG-*JWST* galaxies (stars) and spectroscopically confirmed blue monsters (diamonds). The sources are color-coded by redshift ‘ z ’. The orange shaded region shows the minimum value expected for β assuming a standard stellar population with no dust and maximum nebular contribution to the emission as described in Cullen et al. 2024. *Bottom:* The Balmer decrement $H\delta/H\beta$ of the BoRG-*JWST* galaxies (stars) shows that the line ratios are in agreement within $1\text{-}\sigma$ to the intrinsic value assuming case B recombination in Osterbrock & Ferland (2006).

and 84th percentiles as lower and upper bounds on the uncertainty, respectively, of all these best-fit parameters.

3. RESULTS AND DISCUSSION

Below we present results on the analysis of the BoRG-*JWST* galaxies that confirm their analog nature to $z \gtrsim 10$ blue monsters. For comparison, we include the galaxies Gz9p3 at $z = 9.3127$ (Castellano et al. 2023; Boyett et al. 2024); GN-z9p4 at $z = 9.380$ (Schaerer et al.

2024); GHZ1 at $z = 9.875$, GHZ8 at $z = 10.231$ and GHZ7 at $z = 10.43$ (Napolitano et al. 2025); GN-z11 at $z = 10.603$ (Oesch et al. 2016; Bunker et al. 2023); GHZ2 at $z = 12.34$ (Castellano et al. 2022, 2024); JADES-GS-z14-0 at $z = 14.32$ (Carniani et al. 2024), and MoM-z14 at $z = 14.44$ (Naidu et al. 2025).

3.1. Lack of dust extinction

The β_{UV} continuum slope is a sensitive probe of dust attenuation and stellar populations when direct measurements of dust content are not available. As an example, Cullen et al. (2024) performed an analysis of the β_{UV} slope in photometric samples of $z \gtrsim 8$ galaxies using an extended wavelength baseline afforded by the combination of *JWST*/NIRCam and COSMOS/UltraVISTA. Their analysis on the evolution of β_{UV} with redshift showed that $z > 10.5$ galaxies had on average values of $\beta_{UV} \gtrsim -2.4$, in agreement with values attributable to standard stellar populations with minimum dust content and maximum contribution of the nebular continuum to the emission of these galaxies (e.g., Cullen et al. 2017; Reddy et al. 2018). However, several galaxies at higher redshifts display slopes bluer than the $\beta_{UV} \sim -2.6$ limit for star-forming galaxies with negligible dust attenuation (Chisholm et al. 2022), thus questioning the mechanisms producing the UV continuum emission in blue monsters.

Here we have the opportunity to spectroscopically verify measurements of β_{UV} in the most luminous galaxies at $z \sim 7 - 9$, reducing potential biases in the measurements from photometric scatter and possible emission line contributions. We take the β_{UV} continuum slope values measured by RB25 and plot them as blue stars in the top panel of Figure 1, also adding the measurements of the blue monsters color-coded by redshift. We find that both populations of galaxies tend to be dust-deficient within errors with the lowest cases consistent with the extreme $\beta_{UV} \gtrsim -2.6$ value.

The spectroscopic BoRG-*JWST* data set affords a unique and practical opportunity to verify the “no-extinction” hypothesis proposed to explain the extreme UV luminosities of the $z > 10$ galaxy population. The “Balmer decrement” has proven to be an efficient method to infer the dust content of galaxies (e.g., Glazebrook et al. 1999; Reddy et al. 2008; Madau & Dickinson 2014; Shapley et al. 2003; Sandles et al. 2024). The intrinsic ratios of relevant Balmer lines are calculated under ideal conditions of a dust-free gas cloud, assuming Case B recombination and a typical temperature of $\sim 10,000$ K (Osterbrock 1989; Osterbrock & Ferland 2006). Although the Balmer decrement is traditionally estimated from the brightest Hydrogen Balmer lines $H\alpha/H\beta$, the $H\alpha$ line is redshifted out of the NIRSpect observations, while the prism’s low spectral resolution ($R \sim 100$) prevents us from resolving $H\gamma$ emission from the auroral $[O\text{III}]\lambda 4363$ emission line. Thus, we rely on the $H\delta/H\beta$ ratio for our Balmer decrement analysis.

We use the nebular emission line analysis code PyNeb (Luridiana et al. 2015) to calculate the intrinsic values of the $H\delta/H\beta$ ratio following the Case B recombination.

The code uses the line emissivity intensities from Storey & Hummer (1995) and we adapt electron densities in the range 10^{1-6} cm^{-3} and temperatures $5,000 - 20,000$ K. This yields intrinsic values for $H\delta/H\beta = 0.251 - 0.266$. The measured Balmer ratios for the BoRG-*JWST* galaxies with detected $H\delta$ and $H\beta$ emission at $S/N > 2.5$ are presented in Table 1. We show these ratios as a function of stellar mass $\log M_*/M_\odot$ in the bottom panel of Figure 1, with the intrinsic ratios highlighted in red. The BoRG-*JWST* galaxies used in this analysis are consistent within $1-\sigma$ of the theoretical ratios calculated, confirming little to no dust reddening. There is no evidence of correlation with galaxy mass. The Balmer decrement further supports the hypothesis of negligible dust extinction in the BoRG-*JWST* sample. While such confirmations do not preclude dust production at such early times, the virtually dust-free interstellar medium (ISM) conditions presented here suggest that some mechanism is required to either destroy the dust grains or have them ejected from the ISM for them to remain undetected.

3.2. Nature of the sources: AGN- vs. SF-powered

One of the suggestions to explain such efficient dust depletion in hyper-luminous galaxies is through ejection by outflows from either strong UV radiation pressure of young, massive metal-poor stars, or from an AGN (Ziparo et al. 2023).

Previous work on the selection of BoRG sources utilized morphological analyses to either limit or exclude obvious AGN. Morishita et al. (2020) characterized the expected number density of quasar-like point sources from pure-parallel observations, suggesting $> 100\times$ survey volumes were required to identify quasar-like objects of comparable luminosities to the UV-selected galaxies. Other studies instead applied more direct efforts such as stellarity cuts to exclude the most obvious AGN (Trenti et al. 2011; Calvi et al. 2016; Rojas-Ruiz et al. 2020; Bagley et al. 2024), potentially at the cost of sample completeness.

Once again, despite the challenging endeavour of identifying AGNs, the BoRG-*JWST* spectra provide us with direct measurements to test for obvious spectral signatures of AGN and the theory of dust-ejection by AGN-driven winds. Traditional “BPT” diagrams rely on the detection of strong $H\alpha \lambda 6563$ emission (e.g., Baldwin et al. 1981; Kewley et al. 2001; Kauffmann et al. 2003; Feltre et al. 2016), which is beyond the wavelength coverage of NIRSpect at $z > 8$. Rest-frame UV diagnostics from high-ionization such as $C\text{IV} \lambda\lambda 1548, 1550$, $C\text{III}]\lambda 1909$, and $\text{He II} \lambda 1640$ lines provide a useful alternative, however these are mostly undetected in the relatively shallow individual spectra of BoRG-*JWST* and

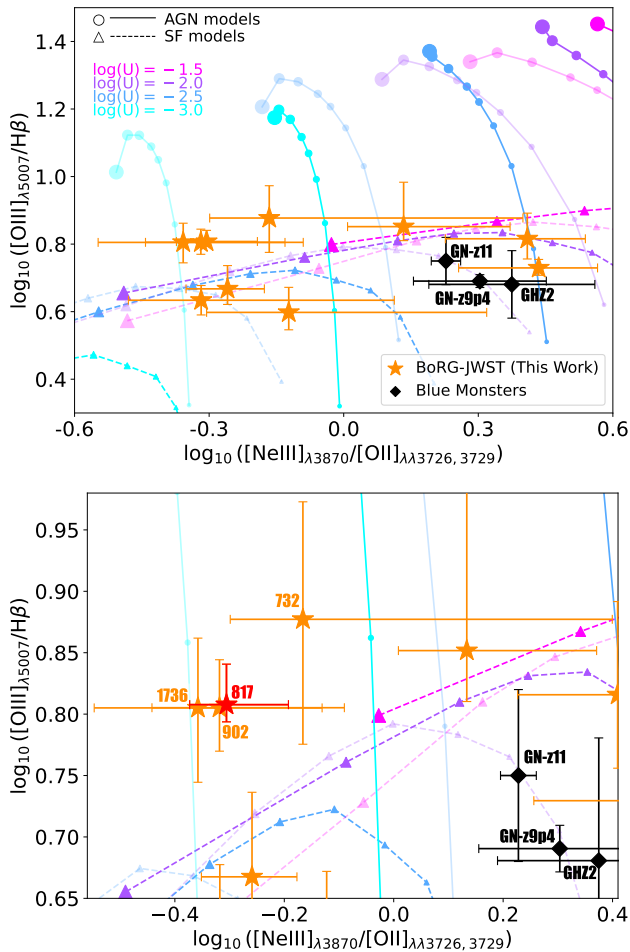


Figure 2. OHNO diagnostic for AGN (contiguous lines with circles) and star-forming galaxies (dashed-lines with triangles). *Top:* The models are color-coded by ionization parameter $\log(U) = [-1.5, -3.0]$ with different color intensities for electron densities $n_e = 10^4 \text{ cm}^{-3}$ (bright) 10^3 cm^{-3} (fainter). The symbols increase in size from subsolar to solar metallicities ($0.05 < Z_{\text{gas}}/Z_{\odot} \leq 1.0$). The measurements for the BoRG-*JWST* galaxies are shown as orange stars and three UV-luminous galaxies at $z > 10$ as black diamonds. *Bottom:* Zoom in of the previous Top figure in the area where AGN solution is more exclusive, although within 1σ (1747_732) and 2σ (1747_902, 2426_1736) of the star forming model solution. Source 1747_817 highlighted in red is marginally consistent with AGN classification, lying 3σ and 7.5σ from star-forming models in the Ne3O2 and R3 directions, respectively.

indeed in most individual high-redshift NIRSspec spectra from the literature.

Nonetheless, a number of useful rest-optical alternatives exist, making use of moderately strong emission lines to differentiate between star-formation and AGN contributions. In particular, we follow the diagnostics showcased by Calabrò et al. (2024) who utilize well-known ratios of $\text{Ne III } \lambda 3870/[\text{O II}] \lambda\lambda 3726, 3729$ (Ne3O2)

vs. $[\text{O III}] \lambda 5007/\text{H}\beta$ (R3), the “OHNO” diagnostic. We present the measured line ratios and uncertainties of our sample in Table 1; galaxies 1747_1081, 2426_1130, 2426_169-n, and 2426_1777 do not have $\text{Ne III } \lambda 3870$ emission detected and are therefore not presented. The OHNO diagnostic plot is shown in Figure 2, where we also plot the AGN models (contiguous lines with circles) and star-forming models (dashed lines with triangles) from Calabrò et al. (2023), for comparison. The models are color-coded by ionization parameter (ranging from $\log U = -3.0$ to -1.5), with two electron densities for each $\log U$, $n_e = 10^4 \text{ cm}^{-3}$ (brighter color) and 10^3 (fainter color). The metallicity is represented by the symbols that increase in size from 0.05 to solar metallicities. We add for reference a few blue monsters for which the relevant emission lines or line ratios have already been measured and reported; GN-z9p4 (Schaerer et al. 2024), GN-z11 (Bunker et al. 2023), and GHZ2 (Calabrò et al. 2024; Zavala et al. 2025).

We find that the BoRG-*JWST* measurements span either the low end of AGN ionization models with $\log U < -2.0$, or virtually the full range of ionization parameters for star-forming models. We find that a subset of these (four sources) possibly prefer the AGN models with low ionization $\log U = -3.0$, as highlighted in Figure 2, bottom. However, the ratios are within 1σ (source 1747_732), or 2σ (1747_902, and 2426_1736) of the star-forming models. Source 1747_817 can marginally be classified as an AGN with this diagnostic given that its Ne3O2 ratio deviates by 3σ from the star-forming model with $\log U = -1.5$, $n_e = 10^4 \text{ cm}^{-3}$, and solar metallicity, while the R3 ratio differs by 7.5σ from the model at $\log U = -2.0$, similar density, and near-solar metallicity $Z_{\text{gas}}/Z_{\odot} \sim 0.7 - 1.0$. A low-ionization AGN is a more plausible explanation than a solar-metallicity star-forming galaxy at $z = 7.556$, although at least one such high-metallicity system has been reported in the literature (see Shapley et al. (2025)).

However, we see no evidence for additional or unambiguous signatures suggesting strong or dominant AGN contributions. All these sources, except for 1747_732, present detection of strong $\text{C III}] \lambda\lambda 1907, 1909$ at $\text{S/N} > 3.0$, with 1747_817 having emission of the blended $[\text{O III}] \lambda 1660, \lambda 1666$ at $\text{S/N} = 5.1$, as is typical for high-redshift star-forming sources (Roberts-Borsani et al. 2024). These emission lines typically trace strong ionization from either low-metallicity stellar population or AGN activity, with their equivalent widths serving as a key diagnostic in conjunction with other, higher-ionization UV lines (e.g., Stark et al. 2017; Nakajima et al. 2018; Fèvre et al. 2019). However, our spectral

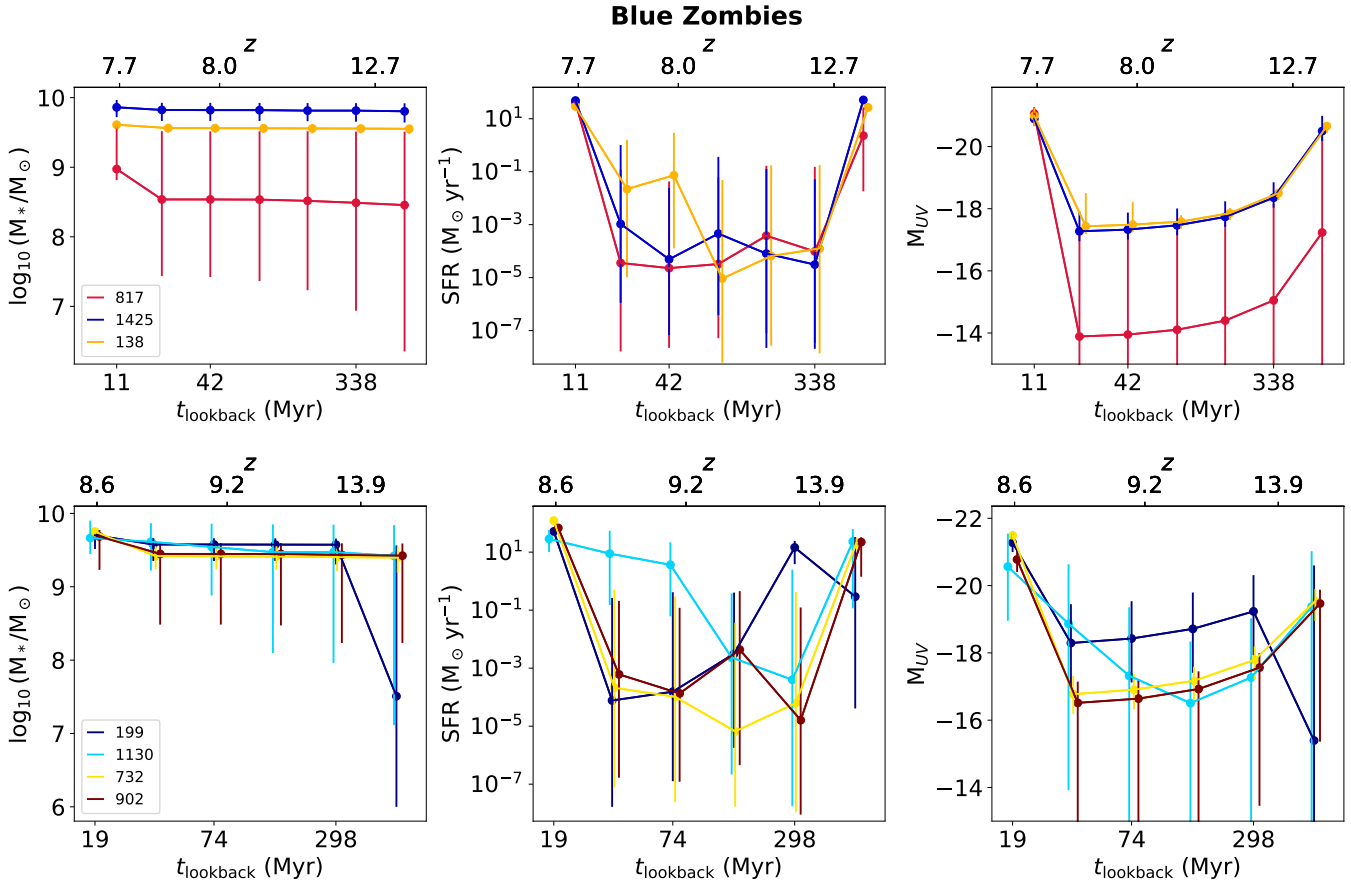


Figure 3. Inferred evolution of the BoRG-*JWST* galaxies using spectral fitting. *Left:* Stellar mass growth as a function of lookback time from the epoch of observation and corresponding redshift. *Center:* Star formation rate, displaying intense bursts of star formation. *Right:* Cumulative M_{UV} luminosity as a function of lookback time/redshift; the gray shaded region shows the limit at which the galaxy approaches $M_{UV} \sim -20$. The galaxies in this first category of “Blue Zombies” are characterized by having a first burst at $z \gtrsim 12$ reaching $M_{UV} \lesssim -20$, lull over time, and then have a recent burst closer to observation ($z \simeq 7-9$).

resolution is insufficient to reliably deblend the components or to robustly estimate the equivalent width.

Thus, while our sample are consistent with the range of star-forming models with low metallicity and strong ionization parameters, we cannot rule out moderate AGN contributions with the present data set. Deeper and higher spectral resolution data will be required for definitive conclusions.

3.3. Bursty Episodes of Star Formation

Stochastic (or “bursty”) star formation histories have been proposed as a key feature to explain the extreme UV luminosities of the blue monsters. These bursty episodes of star formation could arise as a consequence of multiple feedback processes typical in early galaxies ($z > 7$) driven by supernovae (e.g., El-Badry et al. 2016; Mirocha & Furlanetto 2023; Sun et al. 2023) or outflows from stellar winds (e.g., Gelli et al. 2024; Carnall et al. 2023). Based on the model explored by Ferrara (2024a) for JADES-GS-z14-0 at $z = 14.32$, blue monsters have

been suggested to have undergone a short and intense burst of star formation in the last ~ 40 Myr before observation, accompanied by outflows revealing UV-bright and young stellar populations. Before this, other obscured or smoldering bursts of star formation can last 30-40 Myr and are separated by quenching phases of ~ 20 Myrs. Thus, from the birth of the first stars, star formation and thus the stellar mass increases with time in patches rather than smoothly. These bursts in the evolution should be identifiable in the SFH, however constraints from the rest-frame optical—where longer-lived stars emit the majority of their light—are fundamental for accurate constraints (e.g., Witten et al. 2025) over more extended timescales. At $z \gtrsim 10$, such constraints are beyond the wavelength range of NIRSpect and NIRCAM, and impractical with MIRI, highlighting the usefulness of the hyper-luminous BoRG-*JWST* objects at $z \simeq 7-9$.

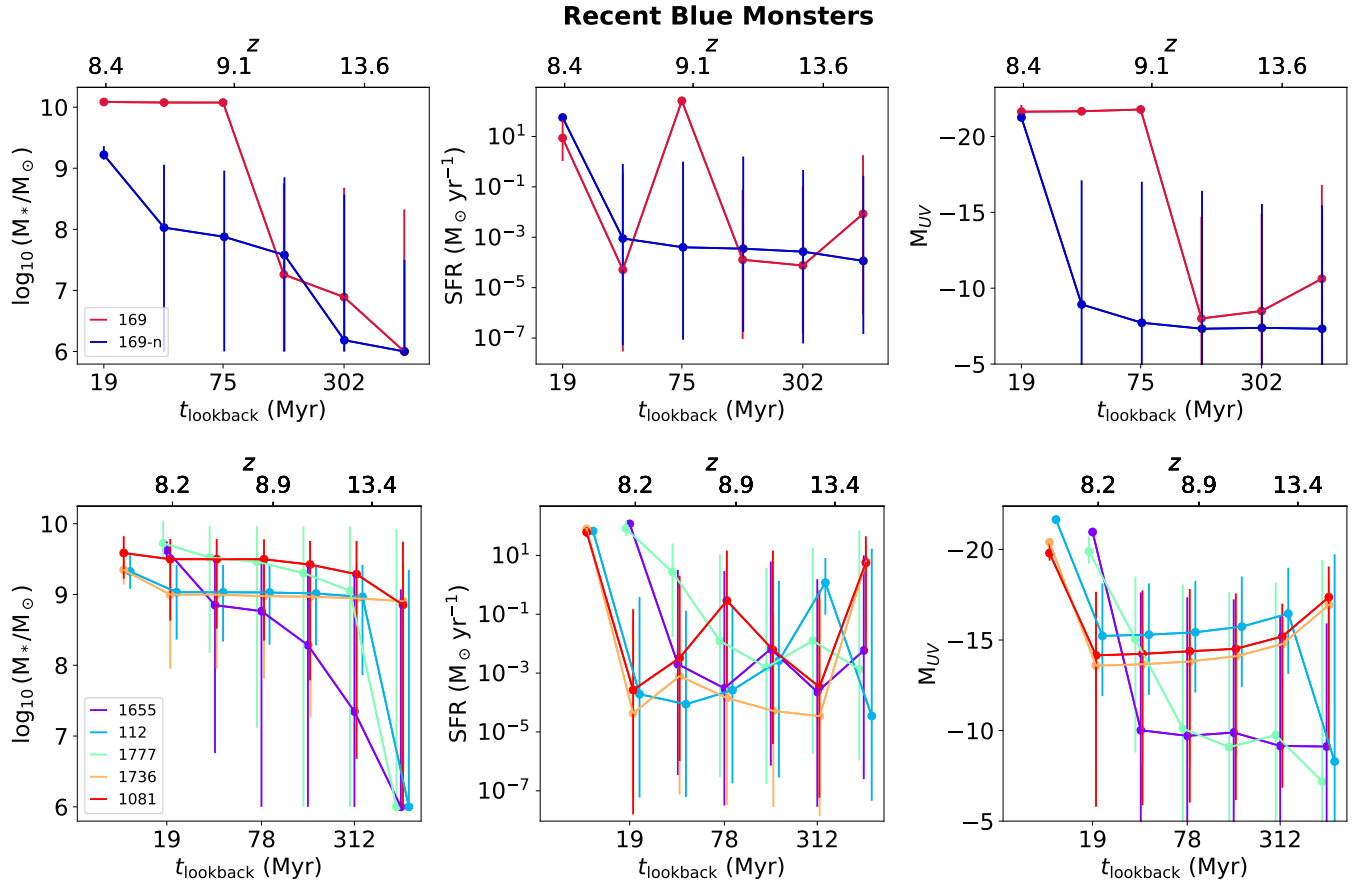


Figure 4. Same as Figure 3 for the other half of the sample denominated “Recent Blue Monsters” characterized by a recent burst in star formation reaching a brightness $M_{UV} \lesssim -20$ closer to observation.

With rest-UV-to-optical spectra in hand, we model the SFH of the BoRG-*JWST* sample using the *gsf* spectral fitting code, to identify the presence (or otherwise) of bursty episodes of star formation. In Figures 3 and 4 we present the stellar mass, star formation rate, and cumulative M_{UV} as a function of lookback time for each of the BoRG-*JWST* galaxies. We group the results into two categories according to the redshift at which the first burst surpasses the $M_{UV} \sim -20$ brightness. In the first category –named “Blue Zombies” because they become blue monsters a first time, they fade, and then become blue monsters again (Figure 3.3)– we find that half the galaxy sample undergoes a burst within the first 300 Myr of formation, corresponding to $z \gtrsim 12$: 1747_817, 1747_1425, 1747_138, 1747_199, 2426_1130, 1747_732, and 1747_902. This early burst builds up substantial stellar masses of $\log_{10} M_*/M_\odot \gtrsim 8$, which then continue to grow smoothly until a second burst occurs within the final 20 Myr before observation, which agrees with the evolutionary model proposed by Ferrara (2024a).

In the second category –named “Recent Blue Monsters”– is the rest of the sample that is dominated by recent bursts within 20 Myrs of the time of observation (see Figure 4). A special case is galaxy 2426.169 which experiences a very strong ($260 M_\odot \text{ yr}^{-1}$) first burst after ~ 530 Myr ($z \sim 9.1$). After the burst, the star formation rate declines but the galaxy remains bright $M_{UV} < -20$, aided by a secondary burst closer to the time of observations. This case shows how the effects of multiple bursts can contribute to the observed UV luminosity, as proposed by e.g., Mason et al. (2023); Narayanan et al. (2024). Unsurprisingly, this galaxy reaches the largest stellar mass in the sample at $\log_{10} M_*/M_\odot = 10.09^{+0.03}_{-0.04}$, and brightest luminosity $M_{UV} = -22.34 \pm 0.06$. This galaxy was proposed as a neighbor in the same environment of galaxy 2426_169-n (Rojas-Ruiz et al. 2025). Evaluating the SFH of both galaxies, we find they are remarkably different with 2426.169-n having a smooth evolution and no significant changes at the same lookback time as the strong starburst for 2426_169 (see Figure 4, Top panel).

Interestingly, galaxies 1747_112, 1747_817, 2426_1736, 2426_1655, and 2426_169-n have evidence for the most recent burst to have high specific star formation rates (sSFR) exceeding 25 Gyr^{-1} , which is compatible with the scenario by Ferrara 2024b advocating for dust ejection via radiation pressure through a dust-driven outflow. Galaxy 1747_817 has the highest sSFR in the sample at $\text{sSFR} = 45_{-18}^{+111} \text{ Gyr}^{-1}$, in agreement with galaxy JADES-GS-z14-0 (Ferrara 2024a). The analysis presented here, utilizing constraints from both the rest-frame UV to optical, confirm the bursty nature of the hyper-luminous galaxy population, whose stochasticity clearly serve to temporarily and periodically enhance their UV luminosities to extreme levels.

3.4. Conclusions

The analysis on the BoRG-*JWST* $z \sim 8$ galaxies presented here helps to reconstruct the puzzle of the $z \gtrsim 10$ UV-luminous galaxies found with *JWST*. We have the unique opportunity of accessing the rest-optical emission of these galaxies to make predictions on the properties of the $z \gtrsim 10$ blue monsters. Our main results can be summarized as follows:

1. The BoRG-*JWST* galaxies are consistent with having negligible dust extinction, based on the β_{UV} slope and Balmer decrement.
2. We find no strong evidence for AGN activity based on the emission lines available, although some contribution from four sources cannot be ruled out, with one of them (1747_817) being marginally consistent with an AGN in the OHNO diagnostic. Otherwise, both strong star formation and AGN contributions are consistent with the data.
3. Half of the BoRG-*JWST* galaxies have experienced an early burst of star formation at $z > 12$, after which they appeared briefly as “Blue Monsters”, then faded, and then experienced a second major burst shortly before the time of obser-

vations. We call these galaxies “Blue Zombies”. The other half are caught shortly after their main burst of star formation, and are thus named “Recent blue monsters”

Given the similarity between BoRG-*JWST* galaxies and “blue monsters”, we suggest that the same interpretation can be applied to the bright $z \gtrsim 10$ population. In other words, they could be “Blue zombies” caught during their first major burst of star formation.

An important factor that deserves further investigation is the role of environment. The BoRG-*JWST* sample was selected from random pointing in the sky as part of a random pointing survey. At the moment, there is insufficient information to measure environmental parameters such as galaxy overdensity or halo mass. Precise environment measures for the BoRG-*JWST* sample and the “blue monsters” are needed to make progress on this front.

ACKNOWLEDGMENTS

This work is based on observations made with the NASA/ESA/CSA James Webb Space Telescope. The data were obtained from the Mikulski Archive for Space Telescopes at the Space Telescope Science Institute, which is operated by the Association of Universities for Research in Astronomy, Inc., under NASA contract NAS 5-03127 for *JWST*. The specific observations analyzed can be accessed via [doi: 10.17909/9s79-m291](https://doi.org/10.17909/9s79-m291). These observations are associated with programs # 1747 and 2426. Funding from NASA through STScI awards JWST-GO-01747 and JWST-GO-02426 is gratefully acknowledged.

Facilities: *JWST*

Software: Astropy (The Astropy Collaboration et al. 2013), *gsf* (Morishita et al. 2019), Matplotlib (Hunter 2007), Numpy (Harris et al. 2020), SciPy (Virtanen et al. 2020), PyNeb (Luridiana et al. 2013)

REFERENCES

- Bagley, M. B., Finkelstein, S. L., Rojas-Ruiz, S., et al. 2024, *ApJ*, 961, 209
- Bakx, T. J. L. C., Zavala, J. A., Mitsuhashi, I., et al. 2023, *MNRAS*, 519, 5076
- Baldwin, J. A., Phillips, M. M., & Terlevich, R. 1981, *PASP*, 93, 5
- Boyett, K., Trenti, M., Leethochawalit, N., et al. 2024, *NatAs*, 8, 657
- Bunker, A. J., Saxena, A., Cameron, A. J., et al. 2023, *A&A*, 677, A88
- Calabrò, A., Pentericci, L., Feltre, A., et al. 2023, *A&A*, 679, A80
- Calabrò, A., Castellano, M., Zavala, J. A., et al. 2024, *ApJ*, 975, 245
- Calvi, V., Trenti, M., Stiavelli, M., et al. 2016, *ApJ*, 817, 120

- Carnall, A. C., Begley, R., McLeod, D. J., et al. 2023, *MNRAS*, 518, L45
- Carniani, S., Hainline, K., D'Eugenio, F., et al. 2024, *Natur*, 633, 318
- Carniani, S., D'Eugenio, F., Ji, X., et al. 2025, *A&A*, 696, A87
- Casey, C. M., Akins, H. B., Shuntov, M., et al. 2024, *ApJ*, 965, 98
- Castellano, M., Fontana, A., Treu, T., et al. 2022, *ApJ*, 938, L15
- Castellano, M., Fontana, A., Treu, T., et al. 2023, *ApJ*, 948, L14
- Castellano, M., Napolitano, L., Fontana, A., et al. 2024, *ApJ*, 972, 143
- Chabrier, G. 2003, *PASP*, 115, 763
- Chisholm, J., Saldana-Lopez, A., Flury, S., et al. 2022, *MNRAS*, 517, 5104
- Conroy, C., Gunn, J. E., & White, M. 2009, *ApJ*, 699, 486
- Cullen, F., McLure, R. J., Khochfar, S., Dunlop, J. S., & Dalla Vecchia, C. 2017, *MNRAS*, 470, 3006
- Cullen, F., McLeod, D. J., McLure, R. J., et al. 2024, *MNRAS*, 531, 997
- Curtis-Lake, E., Carniani, S., Cameron, A., et al. 2023, *NatAs*, 7, 622
- Dressler, A., Vulcani, B., Treu, T., et al. 2023, *ApJ*, 947, L27
- Dressler, A., Rieke, M., Eisenstein, D., et al. 2024, *ApJ*, 964, 150
- El-Badry, K., Wetzel, A., Geha, M., et al. 2016, *ApJ*, 820, 131
- Feltre, A., Charlot, S., & Gutkin, J. 2016, *MNRAS*, 456, 3354
- Ferrara, A. 2024a, *A&A*, 689, A310
- Ferrara, A. 2024b, *A&A*, 684, A207
- Ferrara, A., Pallottini, A., & Dayal, P. 2023, *MNRAS*, 522, 3986
- Ferrara, A., Pallottini, A., & Sommovigo, L. 2025, *A&A*, 694, A286
- Finkelstein, S. L., Bagley, M. B., Arrabal Haro, P., et al. 2022, *ApJ*, 940, L55
- Finkelstein, S. L., Bagley, M. B., Ferguson, H. C., et al. 2023, *ApJL*, 946, L13
- Finkelstein, S. L., Leung, G. C. K., Bagley, M. B., et al. 2024, *ApJL*, 969, L2
- Fiore, F., Ferrara, A., Bischetti, M., Feruglio, C., & Travascio, A. 2023, *ApJL*, 943, L27
- Foreman-Mackey, D., Hogg, D. W., Lang, D., & Goodman, J. 2013, *PASA*, 125, 306
- Fujimoto, S., Finkelstein, S. L., Burgarella, D., et al. 2023, *ApJ*, 955, 130
- Fèvre, O. L., Lemaux, B. C., Nakajima, K., et al. 2019, *A&A*, 625, A51
- Gelli, V., Mason, C., & Hayward, C. C. 2024, *ApJ*, 975, 192
- Glazebrook, K., Blake, C., Economou, F., Lilly, S., & Colless, M. 1999, *MNRAS*, 306, 843
- Hainline, K. N., Johnson, B. D., Robertson, B., et al. 2024, *ApJ*, 964, 71
- Harikane, Y., Ouchi, M., Oguri, M., et al. 2023, *ApJS*, 265, 5
- Harris, C. R., Millman, K. J., van der Walt, S. J., et al. 2020, *Nature*, 585, 357
- Hsiao, T. Y.-Y., Abdurro'uf, Coe, D., et al. 2024, *ApJ*, 973, 8
- Hunter, J. D. 2007, *CSE*, 9, 90, conference Name: Computing in Science Engineering
- Kauffmann, G., Heckman, T. M., Tremonti, C., et al. 2003, *MNRAS*, 346, 1055
- Kewley, L. J., Dopita, M. A., Sutherland, R. S., Heisler, C. A., & Trevena, J. 2001, *ApJ*, 556, 121
- Luridiana, V., Morisset, C., & Shaw, R. A. 2013, *Astrophysics Source Code Library*, ascl:1304.021
- Luridiana, V., Morisset, C., & Shaw, R. A. 2015, *A&A*, 573, A42
- Madau, P., & Dickinson, M. 2014, *ARA&A*, 52, 415
- Maiolino, R., Scholtz, J., Witstok, J., et al. 2024a, *Natur*, 630, E2
- Maiolino, R., Scholtz, J., Witstok, J., et al. 2024b, *Natur*, 627, 59
- Mason, C. A., Trenti, M., & Treu, T. 2023, *MNRAS*, 521, 497
- Mirocha, J., & Furlanetto, S. R. 2023, *MNRAS*, 519, 843
- Morishita, T., Abramson, L. E., Treu, T., et al. 2019, *ApJ*, 877, 141
- Morishita, T., Stiavelli, M., Trenti, M., et al. 2020, *ApJ*, 904, 50
- Naidu, R. P., Oesch, P. A., van Dokkum, P., et al. 2022, *ApJL*, 940, L14
- Naidu, R. P., Oesch, P. A., Brammer, G., et al. 2025, 2025arXiv250511263N
- Nakajima, K., Schaerer, D., Le Fèvre, O., et al. 2018, *A&A*, 612, A94
- Napolitano, L., Castellano, M., Pentericci, L., et al. 2024, 2024arXiv241018763N
- Napolitano, L., Castellano, M., Pentericci, L., et al. 2025, *A&A*, 693, A50
- Narayanan, D., Lower, S., Torrey, P., et al. 2024, *ApJ*, 961, 73
- Oesch, P. A., Brammer, G., Dokkum, P. G. v., et al. 2016, *ApJ*, 819, 129

- Osterbrock, D. E. 1989, *Astrophysics of gaseous nebulae and active galactic nuclei*, publication Title: *Astrophysics of Gaseous Nebulae and Active Galactic Nuclei*
- Osterbrock, D. E., & Ferland, G. J. 2006, *Astrophysics of gaseous nebulae and active galactic nuclei*
- Reddy, N. A., Steidel, C. C., Pettini, M., et al. 2008, *ApJS*, 175, 48
- Reddy, N. A., Oesch, P. A., Bouwens, R. J., et al. 2018, *ApJ*, 853, 56, publisher: The American Astronomical Society
- Roberts-Borsani, G., Treu, T., Shapley, A., et al. 2024, *ApJ*, 976, 193
- Roberts-Borsani, G., Bagley, M., Rojas-Ruiz, S., et al. 2025, *ApJ*, 983, 18
- Robertson, B., Johnson, B. D., Tacchella, S., et al. 2024, *ApJ*, 970, 31
- Rojas-Ruiz, S., Finkelstein, S. L., Bagley, M. B., et al. 2020, *ApJ*, 891, 146
- Rojas-Ruiz, S., Bagley, M., Roberts-Borsani, G., et al. 2025, *ApJ*, 985, 80
- Sandles, L., D'Eugenio, F., Maiolino, R., et al. 2024, *A&A*, 691, A305
- Schaerer, D., Marques-Chaves, R., Xiao, M., & Korber, D. 2024, *A&A*, 687, L11
- Shapley, A. E., Steidel, C. C., Pettini, M., & Adelberger, K. L. 2003, *ApJ*, 588, 65
- Shapley, A. E., Sanders, R. L., Topping, M. W., et al. 2025, *ApJ*, 981, 167
- Stark, D. P., Ellis, R. S., Charlot, S., et al. 2017, *MNRAS*, 464, 469
- Storey, P. J., & Hummer, D. G. 1995, *MNRAS*, 272, 41
- Sun, G., Faucher-Giguère, C.-A., Hayward, C. C., et al. 2023, *ApJL*, 955, L35
- The Astropy Collaboration, Robitaille, T. P., Tollerud, E. J., et al. 2013, *A&A*, 558, A33
- Trenti, M., Bradley, L. D., Stiavelli, M., et al. 2011, *ApJ*, 727, L39
- Virtanen, P., Gommers, R., Oliphant, T. E., et al. 2020, *NatMe*, 17, 261
- Witten, C., McClymont, W., Laporte, N., et al. 2025, *MNRAS*, 537, 112
- Zavala, J. A., Castellano, M., Akins, H. B., et al. 2025, *NatAs*, 9, 155
- Ziparo, F., Ferrara, A., Sommovigo, L., & Kohandel, M. 2023, *MNRAS*, 520, 2445
- Álvarez Márquez, J., Crespo Gómez, A., Colina, L., et al. 2025, *A&A*, 695, A250